VII International Conference on Computational Methods in Marine Engineering
MARINE 2017
M. Visonneau, P. Queutey and D. Le Touzé (Eds)

ON THE PREDICTION OF SHEAR-LAYER FLOWS WITH RANS AND SRS MODELS

G. Vaz[1], F.S. Pereira[1,2,3] and L. Eça[3]

[1]Maritime Research Institute Netherlands, Wageningen, the Netherlands

[2]Texas A&M University, College Station, United States of America

[3]Instituto Superior Técnico, Lisbon, Portugal

Key words: Reynolds-Averaged Navier-Stokes equations; Scale-Resolving Simulations; Modelling accuracy; Shear-layer flows; Cylinder flows.

Abstract. This study evaluates the ability of Reynolds-Averaged Navier-Stokes (RANS) and Scale-Resolving Simulations (SRS) models to predict turbulent shear-layer predominant (blunt-body) flows. The selected cases are the flows around a circular cylinder at $Re = 3,900$ and $140,000$, and past a rounded square prism at $Re = 100,000$ and incidence angles of 0 and 45 degrees. These cases exhibit complex features making numerical predictions a challenge, in particular, for turbulence modelling: shear-layers (free, boundary and wake), laminar-turbulent transition, low to moderate Reynolds numbers, flow separation and unsteadiness. In this paper, the aforementioned cases are simulated employing isotropic and anisotropic RANS, Delayed Detached-Eddy Simulation (DDES), eXtra Large-Eddy Simulation (XLES), and Partially-Averaged Navier-Stokes (PANS) equations. The outcome confirms that traditional isotropic RANS are unable to accurately predict such flows, whereas SRS models can significantly reduce modelling errors. Furthermore, the results show that anisotropic RANS models are an interesting engineering option owing to its compromise between accuracy and cost. Nonetheless, an improvement of the modelling accuracy by both anisotropic RANS and SRS models is inevitably coupled with an increase of the numerical demands.

1 INTRODUCTION

Several flows with relevance to naval and maritime hydrodynamics are characterized by high Reynolds numbers ($Re > 10^5$), laminar-turbulent transition, turbulence, complex and/or blunt geometries that originate shear-layer flows, flow separation, and regions that might be dominated by unsteady phenomena. All these features contribute to hamper the accurate numerical representation of such flows, making turbulence modelling a critical aspect. Although traditional isotropic Reynolds-Averaged Navier-Stokes (RANS) equations are widespread in the maritime community and are relatively affordable for the computational resources available in this scientific field, this approach has a limited modelling accuracy in predicting the aforementioned flows.

Contrary to RANS, where all turbulence scales are modelled and averaged, Scale-Resolving Simulation (SRS) models are able to solve some of the turbulence scales, theoretically increasing the modelling accuracy. However, their correct application cannot be done without understanding their main principles, while their accurate numerical solution may be excessively demanding for some practical applications.

Within these SRS models we emphasize two types: 1) the so-called *hybrid* methods which combine a RANS approach in near-wall regions with a LES model in outer and detached regions (e.g. Detached-Eddy Simulation (DES), Delayed Detached-Eddy Simulation (DDES), Very Large-Eddy Simulation (VLES), Extra Large-Eddy Simulation (XLES)); 2) the so-called *bridging* models, which employ the same turbulence approach in the entire domain, whether or not the equations' filter is constant in space and time (e.g. Partially-Averaged Navier-Stokes (PANS) equations and Partially-Integrated Transport Model (PITM)). Naturally, hybrid and bridging formulations are dependent on the physical resolution and on the quality of the underlying (RANS-based in some cases) turbulence model. In terms of turbulence modelling, several approaches have been developed to improve the turbulence models' accuracy by exploiting, for instance, the non-linearity between the Reynolds stresses and the product of the eddy-viscosity and the strain-rate tensor, or the anisotropy of the turbulent field (e.g the *lag* model, $\overline{v^2} - f$ model, Explicit Algebraic Reynold-Stress Model (EARSM), Reynolds-Stress Model (RSM)). Additionally, whenever laminar-turbulent boundary-layer transition plays a role, and the application of SRS is rather of no use (if the models do not solve turbulence at all in the boundary layer) or too expensive (if the models try to solve the transition-relevant small scales in the boundary layer), modern RANS-based transition models might be an attractive solution (e.g. Local Correlation Transition Model (LCTM), $k - k_l - \omega$, Wilcox 2006).

In the last years substantial amount of work has been published by the authors in order to study, implement and verify some of these models, as well as validate their application for several types of blunt-body flows [3, 16–19, 21, 22, 24]. This paper summarizes some of the findings of these previous studies, and compares the performance of some of these new approaches for typical structures used in the maritime industry. The selected models are RANS supplemented with the isotropic $k - \omega$ Shear-Stress Transport (SST) model [10] with or without the Local Correlation Transition Model (LCTM) [9], RANS in combination with the Explicit-Algebraic Reynolds-Stress Model (EARSM) of [2], DDES [5], XLES [7], and PANS [4]. These models are evaluated on four distinct test-cases: the flow around a circular cylinder at Reynolds numbers equal to $3,900$ and $140,000$, and the flow around a rounded square prism at $Re = 100,000$ and two angles of incidence (0 and 45 degrees)[1]. The reasoning behind the selection of these benchmark cases lies on the complexity of the flow physics, simplicity of gridding, and availability of detailed experimental measurements. All this makes these cases extremely useful to gain insight on the selected models, in order to prepare their application to more industrially relevant flows. Note that in these industrial cases, usually the additional geometrical details simplify/force the flow solution by fixing transition and separation zones. Therefore, such flows are not as complex in terms of flow topology and flow phenomena as these canonical test cases that present geometries with continuous smooth walls. Nonetheless, application of the selected models to industrial applications may become computationally expensive.

[1] Work on a square prism at $Re = 22000$ is ongoing [12].

Detailed Verification and Validation studies have been done for some of the cases tackled here [3, 16–19, 21, 22]. In particular, the following numerical studies have been performed: effect of the computational domain size; influence of boundary conditions and third dimension size; consequences of grid layout; influence of iterative convergence; influence of simulation time and quantification of statistical uncertainty; spatial and temporal resolution and quantification of associated discretization uncertainty[2]; influence of explicit turbulence filter. In this paper, we present only one particular set of all those numerical settings tested.

The paper is organized as follows. Section 2 summarizes briefly the major mathematical approaches employed in the current work. Section 3 describes the problems addressed and the numerical setup used. Thereafter, Section 4 presents and discusses the numerical results, while Section 5 presents the conclusions.

2 MATHEMATICAL MODELS

Consider the existence of an arbitrary filter (implicit or explicit), constant preserving, and commuting with spatial and temporal differentiation. The application of such a filtering operator, which decomposes any dependent quantity Φ into a resolved $\langle\Phi\rangle$ and a modelled ϕ component such that $\Phi = \langle\Phi\rangle + \phi$, to the continuity and momentum equations leads to

$$\frac{\partial\langle V_i\rangle}{\partial x_i} = 0 \ , \tag{1}$$

$$\frac{D\langle V_i\rangle}{Dt} = -\frac{1}{\rho}\frac{\partial\langle P\rangle}{\partial x_i} + \frac{\partial}{\partial x_j}\left[\nu\left(\frac{\partial\langle V_i\rangle}{\partial x_j} + \frac{\partial\langle V_j\rangle}{\partial x_i}\right)\right] + \frac{1}{\rho}\frac{\partial}{\partial x_j}\left(\tau_{ij}(v_i, v_j)\right) \ , \tag{2}$$

where the flow is assumed to be incompressible and single-phase. In the previous equations x_i are the coordinates of a Cartesian coordinate system, V_i are the Cartesian velocity components, P is the pressure, ρ is the fluid density, ν is the kinematic viscosity and $\tau_{ij}(v_i, v_j)$ is a tensor produced by the filtering process that contains the effect of the unresolved flow field ϕ on the resolved velocity components $\langle V_i\rangle$ as a diffusion-like term. In order to model $\tau_{ij}(v_i, v_j)$ the Boussinesq hypothesis is used,

$$\frac{\tau_{ij}(v_i, v_j)}{\rho} = 2\nu_t\langle S_{ij}\rangle - \frac{2}{3}k\delta_{ij} \ , \tag{3}$$

where ν_t is the eddy-viscosity, $\langle S_{ij}\rangle$ the resolved strain-rate tensor, k the modelled turbulence kinetic energy, and δ_{ij} the Kronecker symbol. Equations 1 and 2 are valid for any of the models tested in this work. However, as we will describe below, the meaning of $\langle\Phi\rangle$ and $\tau_{ij}(v_i, v_j)$ of the selected models is significantly different.

2.1 Reynolds-Averaged Navier-Stokes Equations

In the RANS equations for statistically unsteady flows, ensemble averaging is applied to the flow variables and to the continuity and momentum equations. This means that all turbulence

[2]Whenever possible, since for some SRS models numerical and modelling errors are entangled and their independent assessment is not an easy task, if possible at all.

fluctuations are modelled and that the dependent variables are mean flow quantities, i.e. statistics to decompose instantaneous quantities into mean and turbulence components have been done *a priori*.

In RANS, $\tau_{ij}(v_i, v_j)$ are the so-called Reynolds stresses, which are modelled in this work using three different turbulence models: the two-equation $k-\omega$ SST eddy-viscosity model; $k-\omega$ SST model combined with local-correlation transition model $\gamma - Re_\theta$ and the explicit algebraic Reynolds stress model (EARSM) based on the two-equation $k-\omega$ TNT eddy-viscosity model. It must be acknowledged that none of these models was developed to simulate statiscally unsteady flows. Therefore, there is no guarantee that the turbulent diffusion term obtained from these models is sufficient to suppress all turbulent fluctuations so that the computed velocity field corresponds to the mean flow.

2.1.1 $k-\omega$ SST Model

The $k-\omega$ SST model [10] is an isotropic eddy-viscosity model widely used in hydrodynamic applications that solves two transport equations to calculate the turbulence kinetic energy, k, and specific dissipation, ω. The eddy-viscosity is calculated from

$$\nu_t = \frac{a_1 k}{\max\{a_1\omega; \langle S\rangle F_2\}}, \tag{4}$$

where $\langle S\rangle$ stands for the mean flow strain-rate magnitude, a_1 is a constant and F_2 an auxiliary function that is given with the remaining constant and functions of the model in [10].

2.1.2 $\gamma - Re_\theta$ Transition Model

It is well known that the $k-\omega$ SST model does not predict transition at the correct location, see for example [3]. The $\gamma - Re_\theta$ transition model (or Local-Correlation Transition Model, LCTM) [9] is combined with the $k-\omega$ SST model to improve the prediction of transition. The definition of ν_t remains unchanged (equation 4), but the production and dissipation terms of the k transport equation depend on the effective intermitency γ_{eff} that is obtained from γ and γ_{sep}, which is related to separation-induced transition.

2.1.3 $k-\omega$ TNT Explicit Algebraic Reynolds-Stress Model

In the EARSM model by Dol et. al [2] a corrective extra anisotropy tensor, $a_{ij}^{(ex)}$, is added to equation 3,

$$\frac{\tau_{ij}(v_i, v_j)}{\rho} = 2\nu_t\langle S\rangle - \frac{2}{3}k\delta_{ij} - a_{ij}^{(ex)}k\,. \tag{5}$$

The selected EARSM model relies on the $k-\omega$ TNT model [8] that calculates the eddy-viscosity from $\nu_t = \frac{k}{\omega}$.

2.2 Delayed Detached-Eddy Simulation

DDES [5] combines RANS in near-wall regions with an SRS model in outer and detached regions. Therefore, the meaning of the dependent variables changes from mean flow in the RANS

region to spaced filtered flow quantities in the SRS region[3]. As a consequence, statistics must be applied a posteriori to the SRS flow field to obtain the mean flow field, which may not be a trivial exercise if the goal is to perform ensemble averaging.

DDES achieves the change from RANS to an SRS approach by changing the dissipation term of the k transport equation to reduce k and consequently ν_t. This modification of the k transport equation changes the meaning of $\tau_{ij}(v_i, v_j)$ from the Reynold stress in the RANS region to the sub-grid scale stress of the SRS region.

A turbulent length scale, l_t,

$$l_t = l_{RANS} - f_d \max\left\{l_{RANS} - l_{LES}; 0\right\} \ , \tag{6}$$

is introduced in the dissipation term of the k transport equation, where $l_{RANS} = \sqrt{k}/\left(\beta^* \omega\right)$ is the RANS length scale and $l_{LES} = C_{DES}\Delta$ is the LES length scale. C_{DES} is a constant and Δ is the largest cell characteristic length. The blending between the RANS and SRS regions is obtained from the f_d empiric function ($0 \leq f_d \leq 1$) defined as

$$f_d = 1 - \tanh\left[\left(C_{d_1} \frac{\nu_t + \nu}{\kappa^2 d^2 \sqrt{0.5\left(\langle S\rangle^2 + \langle \Omega\rangle^2\right)}}\right)^{C_{d_2}}\right] \ . \tag{7}$$

where $\langle \Omega \rangle$ is the resolved vorticity magnitude, κ is the Von-Kármán constant, d is the wall distance and C_{d_1} and C_{d_2} are constants given in [5].

2.3 Extra Large-Eddy Simulation

XLES [7] uses a similar approach, combining the RANS $k-\omega$ TNT model [8] with an LES k sub-grid scale model. To this end, the turbulent length-scale is defined as

$$l_t = \min\left\{\frac{\sqrt{k}}{\omega}; C_1 \Delta\right\} \ , \tag{8}$$

and the eddy-viscosity by $\nu_t = l_t \sqrt{k}$. In equation 8, C_1 is a constant [7].

2.4 Partially-Averaged Navier-Stokes Equations

PANS uses the same mathematical model for the complete flow field. It relies on a RANS turbulence model and two parameters that define the percentage of the turbulence quantities that is modelled, $f_\Phi = \phi/\Phi$ ($f_\Phi = 1$ corresponds to RANS and $f_\Phi = 0$ to DNS). Determination of mean flow quantities requires the application of statistics *a posteriori*, which is only straightforward to do for time-averaged quantities. In this study we selected the PANS formulation of the $k-\omega$ SST model [17], that uses constant values for f_k and f_ε ($f_\omega = f_\varepsilon / f_k$). Unlike the previous SRS models, this model has no direct dependency on the spatial or temporal resolution, permitting to separate numerical and modelling errors.

[3]The discussion of the effect of ignoring commutation errors is out of the scope of this paper.

3 TEST-CASES AND NUMERICAL SETUP

3.1 Case 1: Circular Cylinder at $Re = 3,900$

The flow around a circular cylinder at $Re = 3,900$ is a common benchmark case for turbulence modelling owing to the low Reynolds number and availability of experimental data. At this Re, a laminar boundary-layer detaches from the cylinder's surface originating a free shear-layer. Laminar-turbulent transition occurs in this shear-layer and the wake is fully turbulent. The reference data used in this work is taken from [13–15]. The computational domain mimics the dimensions of the experimental apparatus of [15], except for the span-wise dimension. It is a rectangular prism defined in a Cartesian coordinate system centred at the cylinder axis. The inlet of the computational domain is located $10D$ upstream of the cylinder, whereas the outlet is $40D$ downstream. The cross-section of the domain is $24D \times 3D$ (height $(L_2)\times$ wide (L_3)). The inlet turbulence intensity, I, is 0.2%.

3.2 Case 2: Circular Cylinder at $Re = 140,000$

The main features of this flow are similar to those of the previous case at $Re = 3,900$. However, as the Re increases, laminar-turbulent transition moves upstream. Although at $Re = 140,000$ transition still occurs in the free shear-layer, it takes place in the vicinity of the cylinder. The experimental studies of [1,14] are used for comparison. The computational domain used in this case is equal to that used for the $Re = 3,900$ case. The exception is the span-wise length, L_3/D, that is reduced to 2.0. The inlet turbulence intensity is equal to that reported in [1], $I = 0.1\%$.

3.3 Cases 3 and 4: Rounded Square Prism at $Re = 100,000$ and $0^o/45^o$ of incidence

These cases are part of the *CFD workshop on Code Validation of High Reynolds Number Flow around a Square Column with Rounded Corners* [6]. The selected cases are the flow around a rounded square prism at $Re = 100,000$ and incidence angles of 0 and 45 degrees. The radius, r, of the rounded corners is 16% of the square length/diameter, D. The experimental measurements were carried out on in a cryogenic wind tunnel with a cross squared section $10D$ wide. The numerical simulations use a computational domain centred on the prism's axis with a cross-section of $10D \times 3D$ ($L_2 \times L_3$). The inlet and outlet boundaries are located $8.3D$ upstream and $88.3D$ downstream the prism's axis. Turbulence intensity is set equal to the experimental value of $I = 0.3\%$.

3.4 Numerical Settings

All cases addressed employed multi-block structured grids, figure 1, with spatial resolutions ranging from 3.0×10^6 to 22.4×10^6 cells. The selected time-steps varied from 6.0×10^{-3} to 1.5×10^{-3} time-units, which guaranteed an instantaneous maximum Courant number smaller than 2.0. The details of the spatial-temporal resolutions chosen for this paper are summarized in table 1.

All numerical simulations started from solutions of a precursor 200 time-units RANS simu-

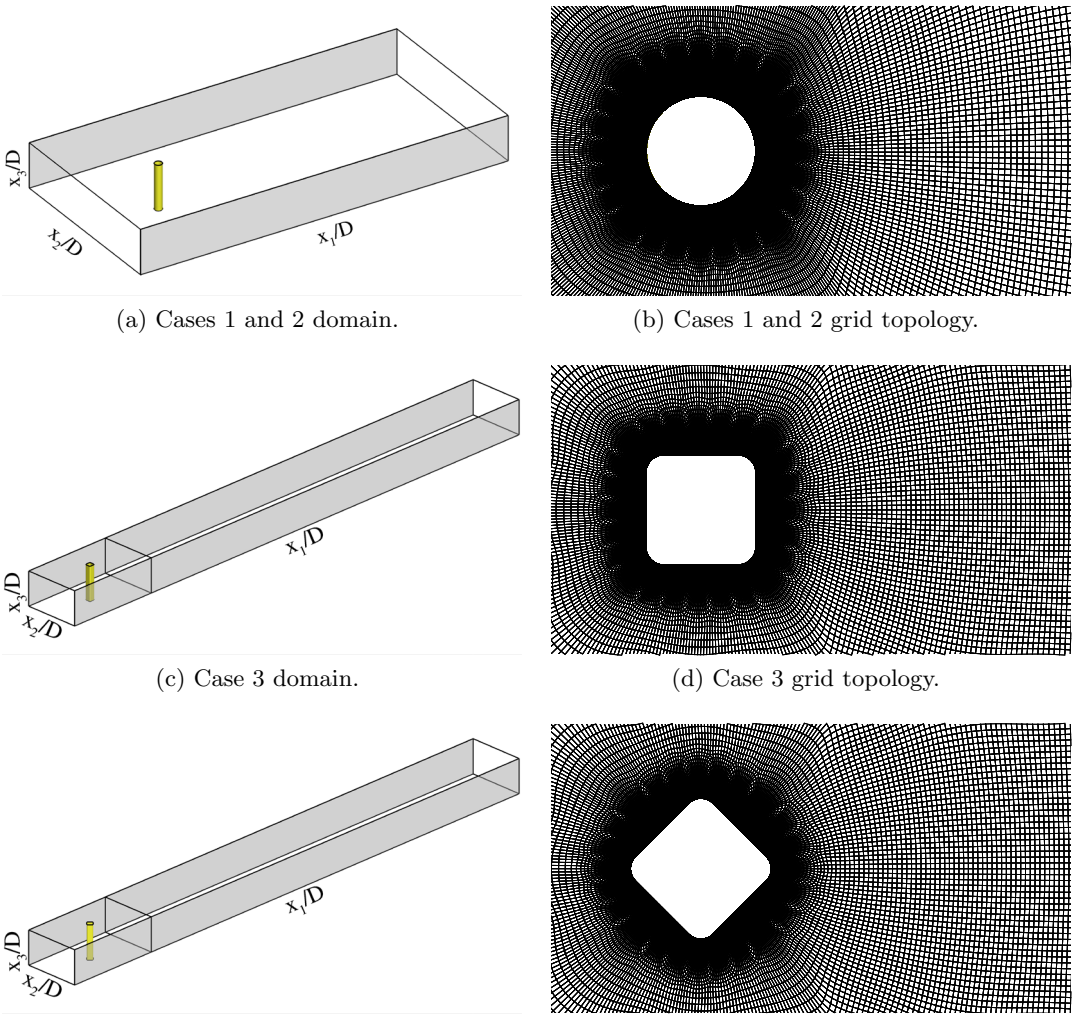

(a) Cases 1 and 2 domain.

(b) Cases 1 and 2 grid topology.

(c) Case 3 domain.

(d) Case 3 grid topology.

(e) Case 4 domain.

(f) Case 4 grid topology.

Figure 1: Computational domain and grid topology of the different cases.

lation. Then, the calculations ran for a period between 200 and 500 time-units[4]. Depending on the case, the first 50 to 100 time-units were discarded. The simulations were carried out in double precision and use an iterative convergence criteria, c_{it}, that requires a maximum normalized residual[5] of 10^{-5} for all transport equations at each time-step. The discretization of the governing equations relied on both temporal and spatial second-order accurate schemes, including the convective terms of all transport equations. Naturally, the mathematical models varied with the test-case. Cases 1 and 2 employed RANS using the SST model with or without the LCTM model (case 2) and the EARSM model (case 1), the hybrid models DDES and XLES

[4]These simulation times are larger than what is normally seen in the literature and have been considered in order to minimize the statistical uncertainty of the results.

[5]Normalized residuals are equivalent to dimensionless variables changes in a simple Jacobi iteration.

and the bridging model PANS solving 75% of the turbulent kinetic energy, K, field ($f_k = 0.25$ and $f_\epsilon = 1.00$). On the other hand, case 3 was simulated with RANS supplemented by SST and EARSM and PANS resolving 50% of K ($f_k = 0.50$ and $f_\epsilon = 1.00$), whereas case 4 relied on RANS using SST and EARSM and DDES. The reasoning for the selection of different models for each case is explained later. All results shown below are normalized[6] by the inflow stream-wise velocity, V_∞, fluid density, ρ and cylinder/prism diameter, D.

Case	L_1/D	L_2/D	L_3/D	N_c	N_3	$\Delta t V_\infty/D$	$\Delta T V_\infty/D$
1	50.0	24.0	3.0	3,011,736	42	5.976×10^{-3}	500
2	50.0	24.0	2.0	22,367,520	240	1.500×10^{-3}	200-500
3	96.7	10.0	3.0	9,384,000	120	2.500×10^{-3}	200-500
4	96.7	10.0	3.0	9,384,000	120	2.500×10^{-3}	200-500

Table 1: Numerical settings of the simulations.

3.5 CFD Code

ReFRESCO (www.refresco.org) is a community based open-usage CFD code for maritime problems. It solves multiphase incompressible viscous-flows using the Navier-Stokes equations (filtered), complemented with turbulence models, cavitation models and volume-fraction transport equations for different phases. The equations are discretized using a finite-volume approach with cell-centred collocated variables, in strong-conservation form, and a pressure-correction equation based on the SIMPLE algorithm is used to ensure mass conservation. Time integration is performed implicitly with first or second-order backward schemes [25]. The implementation is face-based, which permits grids with elements consisting of an arbitrary number of faces and if needed *h-refined* grids. For turbulent flows, RANS and SRS approaches can be used. State-of-the-art CFD features such as moving, sliding and deforming grids, as well automatic grid adaptation (refinement and/or coarsening) are also available. The code is parallelized using MPI and subdomain decomposition, and runs on Linux workstations and HPC clusters. ReFRESCO is currently being developed, verified and applications validated at MARIN (the Netherlands) in collaboration with Instituto Superior Técnico (Portugal), Texas A&M University, and several other universities around the world.

4 RESULTS

4.1 Case 1

The flow around a circular cylinder at $Re = 3,900$ has been addressed in multiple studies as demonstrated in the literature survey presented in [17, 21]. The low Re, simple geometry, and availability of experimental data are the reasons for such interest. The results obtained for the time-averaged drag coefficient, $\overline{C}_D$, base pressure coefficient, $\overline{C}_{pb}$, recirculation length

[6] Reference kinematic viscosity is equivalent to $(V_\infty D)/Re$.

($x_2/D = 0$), $\overline{L}_r$, root-mean-square lift coefficient[7], C'_L, and Strouhal number, St, are presented in table 2.

Model	$\overline{C}_D$	$\overline{C}_{pb}$	$\overline{L}_r$	C'_L	St
SST	1.25	1.36	0.31	0.682	0.217
EARSM	1.06	1.09	0.98	0.348	0.214
DDES	1.01	1.00	1.29	0.238	0.209
XLES	0.95	0.91	1.55	0.127	0.212
PANS	0.94	0.88	1.63	0.112	0.212
Exp.	0.98	0.88	1.51	0.096	0.208

Table 2: Time-averaged drag coefficient, $\overline{C}_D$, base pressure coefficient, $\overline{C}_{pb}$, recirculation length, $\overline{L}_r$, root-mean-square lift coefficient, C'_L, and Strouhal number, St, as a function of the mathematical model. Results for case 1.

The data demonstrates the limitations of traditional isotropic RANS models to predict such class of flows. Except for the St which is reasonably well predicted by all formulations, the SST model leads to large comparison errors, $E_c(\phi) = \phi - \phi_{exp}$. The minimum $E_c(\phi)$ occurs for $\overline{C}_D$ and is larger than 27% of the experimental value. On the other hand, the employment of the EARSM substantially improves the quality of the predictions. The application of SRS models, in turn, further improves the simulations, with the XLES and PANS models attaining an excellent agreement with the experiments.

Integral quantities can be however influenced by modelling errors cancelling and so the assessment of the modelling accuracy based only on these quantities is often biased. Therefore, local quantities have also been analyzed. Time-averaged stream-wise $\langle\overline{V_1}\rangle$ and transverse velocity $\langle\overline{V_2}\rangle$ fields in the near-wake region, as well as pressure distribution on the cylinder's surface, $\overline{C}_p(\theta)$, are shown in figure 2. The results show once more that the SRS approaches, and in this case all of them, present a better agreement with the experimental data than the RANS approaches.

Figure 3 emphasizes the differences between RANS and SRS for the time-averaged cylinder wake field: different circulation zone length, wake axial-velocity deficit and external flow acceleration close to the body which mirrors the different pressure distributions presented in figure 2. Figure 4 presents iso-surfaces of normalized Q (also known as *Q-criterion*), defined as $Q = 1/2\left(\Omega^2/S^2 - 1\right)$ with Ω being the vorticity rate and $S = \langle S\rangle$ the strain rate, for the same instant with respect to lift time history. Results obtained with RANS exhibit three-dimensional effects in the mean flow, which would be obviously missed with a 2-D assumption. Naturally, XLES exhibits totally different flow structures than RANS in the wake due to the instantaneous character of its dependent variables.

4.2 Case 2

The flow around a circular cylinder at $Re = 140,000$ is characterized by transition in the free shear-layer in the vicinity of the cylinder. Considering that the majority of turbulence models was formulated assuming a fully turbulent state and predict transition too early in terms of Reynolds number [3], this case is expected to be challenging. This affects not only the RANS models but also some SRS approaches due to the fact that they do not solve turbulence in the locations where transition occurs (e.g. near-wall regions).

[7]It must be pointed that C'_L may have different meanings in the experiments and in the selected mathematical models.

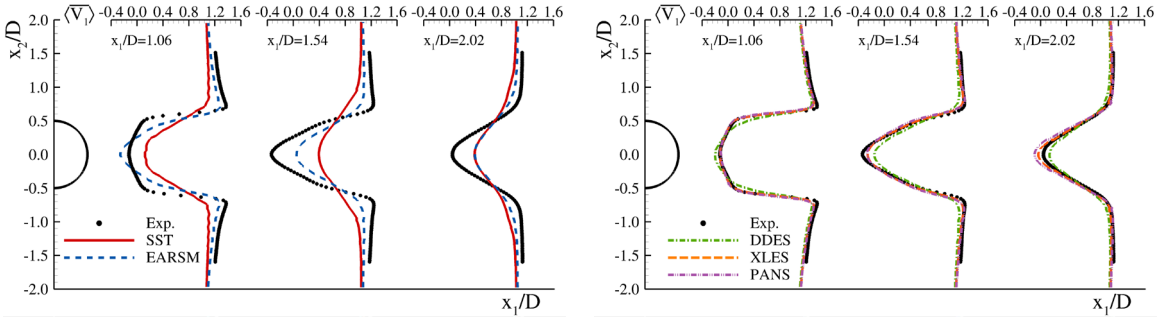

(a) $\langle \overline{V_1} \rangle$ - RANS models. (b) $\langle \overline{V_1} \rangle$ - SRS models.

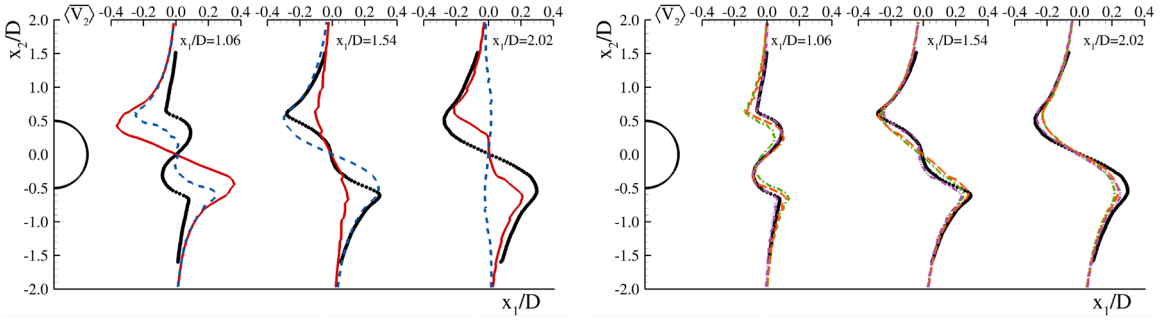

(c) $\langle \overline{V_2} \rangle$ - RANS models. (d) $\langle \overline{V_2} \rangle$ - SRS models.

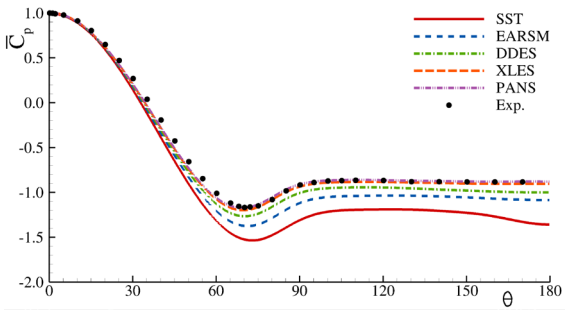

(e) $\overline{C}_p(\theta)$.

Figure 2: Time-averaged stream-wise and transverse velocity, $\langle \overline{V_1} \rangle$ and $\langle \overline{V_2} \rangle$, and pressure distribution on the cylinder's surface, $\overline{C}_p(\theta)$, as a function of the mathematical model. Results for case 1.

The predicted $\overline{C}_D$, $\overline{C}_{pb}$, C'_L, and St are shown in table 3. RANS with SST leads to a poor prediction of the aforementioned quantities. The magnitude of $E_c(\phi)$ is larger than 30% for all the selected quantities. This misrepresentation of the flow is caused by an early transition prediction that occurs in the boundary-layer instead of in the free shear-layer. To further illustrate this point, table 3 has experimental measurements taken at $Re = 5.0 \times 10^6$. It is visible that the RANS/SST predictions match reasonably well with such data. Naturally, this issue is also present in SRS models that do not resolve turbulence in the boundary-layer. Therefore, the

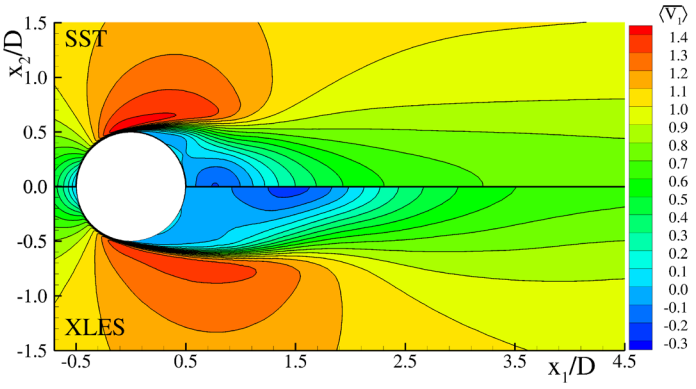

Figure 3: Time-averaged stream-wise velocity, $\langle \overline{V_1} \rangle$, field in the near wake using the SST and XLES models. Results for case 1.

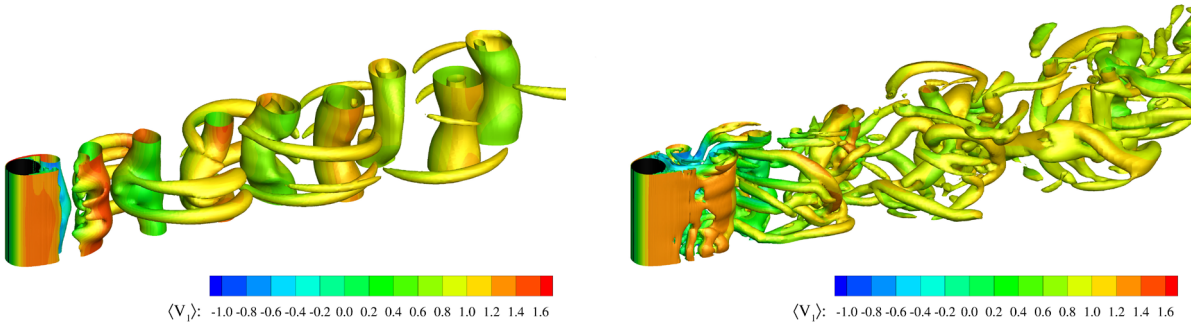

(a) SST. (b) XLES.

Figure 4: Instantaneous Q iso-surfaces ($Q = 0.1$, 0.2 and 0.5) in the near wake using the SST and XLES models. Results for case 1.

results of DDES and XLES show values of $E_c(\phi)$ similar to RANS/SST. On the other hand, the use of LCTM reduces the differences between numerical predictions and experimental data for the selected flow quantities. Furthermore, by resolving a fraction of the turbulent spectrum in the boundary-layer, PANS is able to significantly improve the results. This is also demonstrated in figure 5a for the pressure distribution on cylinder's surface. Whereas PANS achieves low comparison errors, the remaining formulations lead to large values of $E_c(\overline{C}_p(\theta))$.

Figure 5b depicts the stream-wise velocity, $\langle \overline{V}_1 \rangle$, predicted with RANS/SST, LCTM, and PANS. It shows that despite the quality of PANS ($f_k = 0.25$) to predict to quantities given in table 3 and $\overline{C}_p(\theta)$, the time-averaged profile of $\overline{V}_1$ at $x_2/D = 0$ is poorly captured. This deserves further investigation.

Finally, figure 6 presents instantaneous Q iso-surfaces for RANS and PANS solutions. It shows that RANS captures three-dimensional vortical structures in the shear-layer, as for the previous test case. On the other hand, this figure also illustrates the capabilities of a SRS bridging approach like PANS, once the spatial and temporal resolution is fine enough to model the relevant physics of the flow; PANS not only resolves a very large spectrum of turbulence scales in the shear-layer but also in the boundary-layer. This advocates the future use of PANS even for the simulation of boundary-layer transitional flows.

Model	$\overline{C}_D$	$\overline{C}_{pb}$	C'_L	St
SST	0.72	0.83	0.35	0.244
LCTM	1.08	1.24	0.62	0.203
DDES	0.65	0.77	0.03	0.264
XLES	0.68	0.75	0.05	0.264
PANS	1.26	1.32	0.52	0.188
Exp.	1.24	1.21	0.52	0.179
Exp.[2]	0.74	0.93	-	0.257

Table 3: Time-averaged drag coefficient, $\overline{C}_D$, base pressure coefficient, $\overline{C}_{pb}$, recirculation length, $\overline{L}_r$, root-mean-square lift coefficient, C'_L, and Strouhal number, St, as a function of mathematical model. Case 2. Exp.[2] indicates experiments at $Re \approx 5 \times 10^6$ [23].

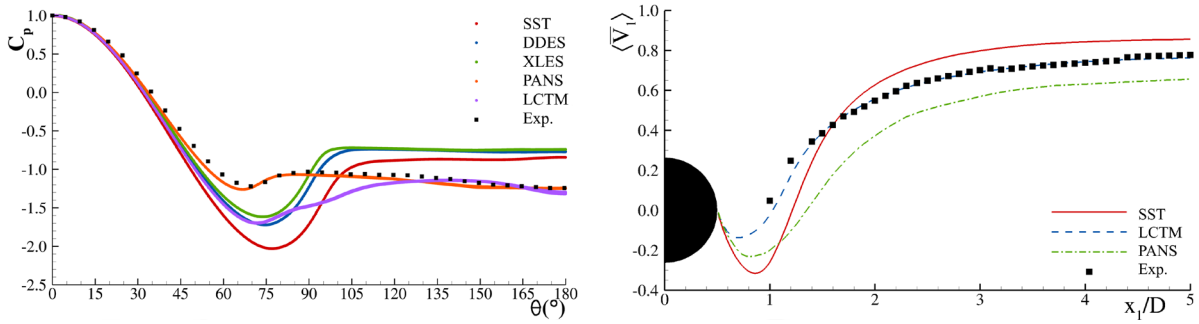

(a) $\overline{C}_p(\theta)$. (b) $\langle \overline{V_1} \rangle$ at $x_2/D = 0.0$.

Figure 5: Time-averaged stream-wise velocity, $\langle \overline{V_1} \rangle$, at $x_2/D = 0.0$, and pressure distribution on the cylinder's surface, $\overline{C}_p(\theta)$, as a function of the mathematical model. Results for case 2.

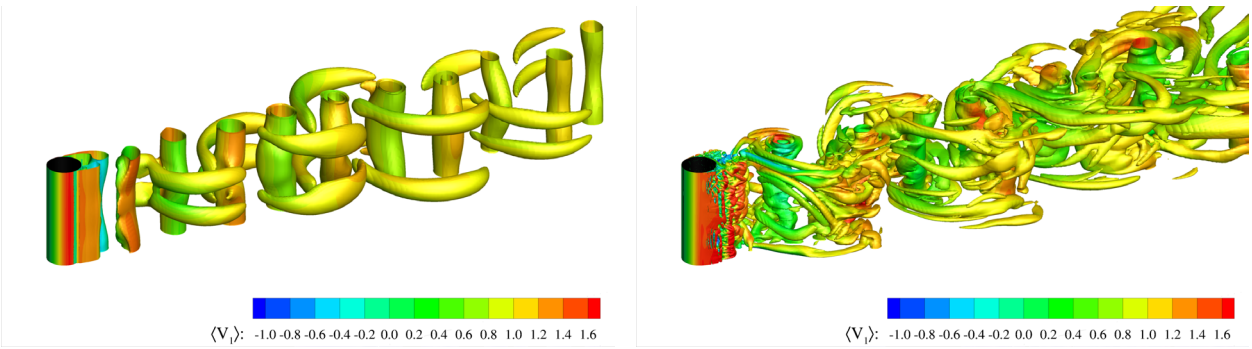

(a) SST. (b) PANS.

Figure 6: Instantaneous Q iso-surfaces ($Q = 0.1$, 0.2 and 0.5) in the near wake using the SST and PANS models. Results for case 2.

4.3 Cases 3 and 4

The last cases addressed in this work are the flows around a rounded square prism at angles of incidence of 0 and 45 degrees. The quantitative results are shown in table 4. The results obtained with RANS using EARSM and DDES/PANS demonstrate a significant reduction of $E_c(\phi)$ when compared to those of the SST model. It is also interesting to observe the similarity

of results between RANS/EARSM and PANS or DDES models. Although experimental results are not available for the time-averaged stream-wise velocity field, $\langle\overline{V_1}\rangle$, in the near-wake, and pressure distribution on the prism's surface, $\overline{C}_p(\theta)$, the data shown in figure 7 presents similar trends between models.

	$\alpha = 0^o$					$\alpha = 45^o$				
Model	$\overline{C}_D$	$\overline{C}_{p_1}$	$\overline{C}_{p_2}$	$\overline{L}_r$	St	$\overline{C}_D$	$\overline{C}_{p_1}$	$\overline{C}_{p_2}$	$\overline{L}_r$	St
SST	1.17	1.18	0.86	2.48	0.159	2.09	0.14	1.96	1.30	0.150
EARSM	1.64	1.56	1.40	0.78	0.158	1.77	0.17	1.65	1.65	0.146
DDES	-	-	-	-	-	1.73	0.19	1.62	1.97	0.134
PANS	1.66	1.58	1.48	0.73	0.146	-	-	-	-	-
Exp.	1.41	1.36	1.13	-	0.142	1.77	0.22	1.60	-	0.168

Table 4: Time-averaged drag coefficient, $\overline{C}_D$, pressure coefficient at two different locations, $\overline{C}_{p_1}, \overline{C}_{p_2}$, recirculation length, $\overline{L}_r$, and Strouhal number, St, as a function of mathematical model. Cases 3 and 4.

It is important to mention the reason why different SRS models are used in cases 3 and 4. The use of a hybrid formulation is advantageous to attain a good trade-off between modelling accuracy and numerical resources, especially for high Reynolds numbers. However, the application of this type of formulation should be avoided if the boundary/shear-layer cannot be modelled accurately by RANS, or in case a critical region of the flow is located in the transition between the RANS and SRS modes. The former issue might occur in case 3 owing to the proximity of the crucial shear-layer to the prism's wall. Consequently, the authors preferred to use a SRS formulation able to resolve turbulence in the near-wall region (PANS) in this case. For case 4, due to the large detached free shear-layer hybrid methods should be adequate.

Figure 8 presents Q iso-surfaces for the RANS/SST and DDES solutions for case 4, zoomed closer to the structure than for the previous cases. The results show that for this 45 degree orientation RANS/SST predicts a shear layer with more three-dimensionality and less vortical coherence than for the previous test cases, especially in the near-wake. Since the boundary-layer detaches from the structure into a large free shear-layer, the DDES model activates its LES character in these layers, permitting to solve turbulence, even if these are close to the body.

4.4 General Remarks

From the previous results and experience on the selected test cases, some general remarks can be made:

- While for cases 1 and 2 the numerical errors seem to be under control, and the spatial and temporal resolutions used adequate for the problems at hand (verification studies have been performed but not shown here) for cases 3 and 4, both grids, time-steps and computational times need further refinement.

- When shear-layers are important, large and even if close to bodies, hybrid SRS approaches are a viable choice to increase the fidelity of the calculations when compared with linear

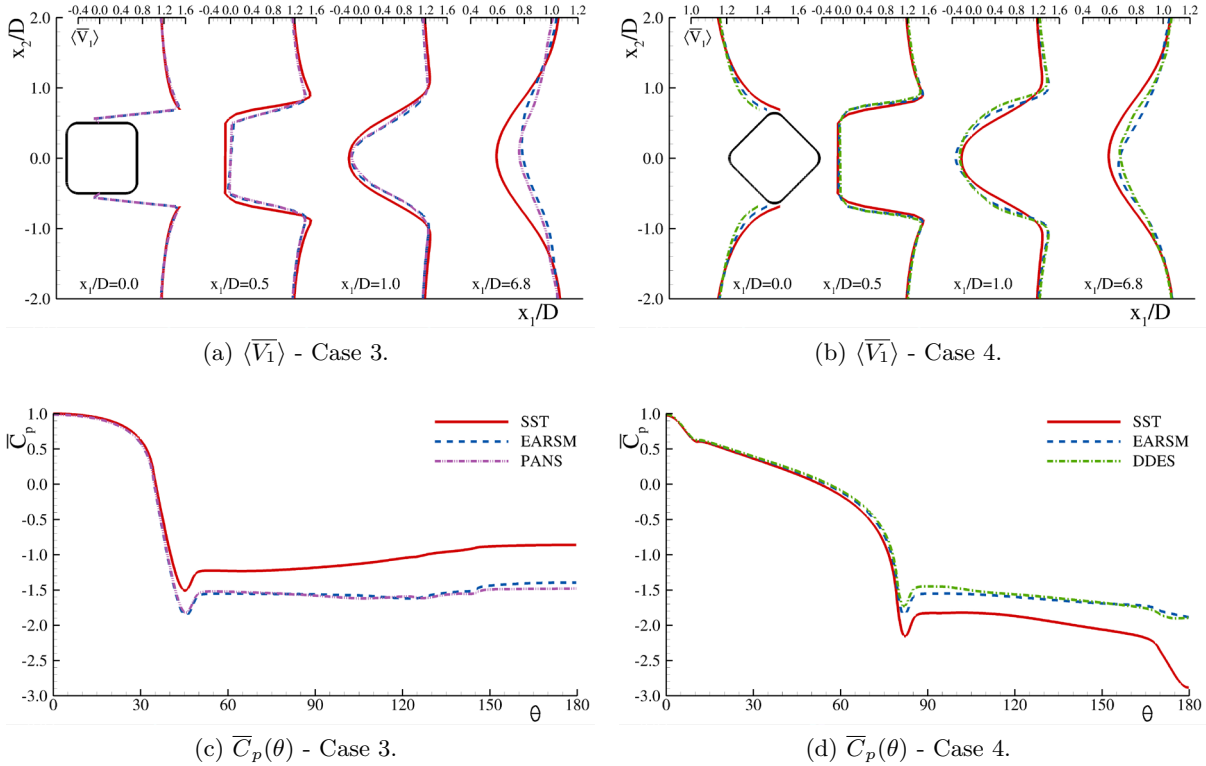

(a) $\langle \overline{V_1} \rangle$ - Case 3.

(b) $\langle \overline{V_1} \rangle$ - Case 4.

(c) $\overline{C}_p(\theta)$ - Case 3.

(d) $\overline{C}_p(\theta)$ - Case 4.

Figure 7: Time-averaged stream-wise velocity, $\langle \overline{V_1} \rangle$, and pressure distribution on the prism's surface, $\overline{C}_p(\theta)$, as a function of the mathematical model. Results for cases 3 and 4.

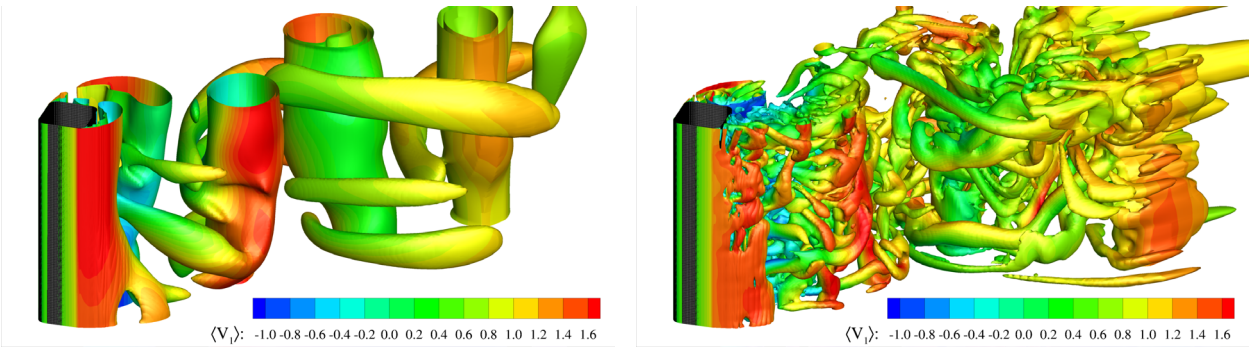

(a) SST.

(b) DDES.

Figure 8: Instantaneous Q iso-surfaces ($Q = 0.1$, 0.2 and 0.5) in the near wake using the SST and DDES models. Results for case 4.

RANS approaches. When laminar-turbulent transition occurs in these layers, and the spatial and temporal resolutions are fine enough, transition might be captured by hybrid SRS methods.

- When laminar-turbulent transition is predicted in the near-wall region (e.g. inside the boundary-layer), hybrid SRS methods will act as RANS and so they suffer from the same problems as the underlying RANS turbulence models. Bridging methods, that solve turbulence also inside the boundary-layer are theoretically more adequate to tackle these problems, at an increasing computational cost. For fully turbulent unsteady boundary layers around blunt bodies, the current linear RANS turbulence models derived for statistically steady flows are not accurate enough. In this situation, both hybrid and bridging models should be applied.

- Ideally, SRS methods should be engineering-safe methods where for coarse temporal and spatial resolutions they should fall back to their RANS formulations. However, for mildly separated/unstable flows DDES/XLES methods may suffer from the well-known "grey-area" problem [11]. For PANS, the results are highly dependent on the filter size f_k, and a wrong combination of grid, time-step and filter may lead to large modelling errors; these cannot be chosen independently of each other, even if numerical and modelling errors are not entangled. This means that a three-dimensional convergence study (filter, grid size and time-step size) is needed to fully assess modelling accuracy, such as done in [21].

- EARSM, being a non-linear RANS model delivered improved accuracy for all cases tested here. The LCTM transition model also improves the modelling of boundary-layer and shear-layer transition when compared with the RANS solution using the underlying turbulence model.

- In terms of computational costs, for the same grid and time-step, table 5 shows the number of iterations per time step, needed to reach the desired maximum normal residual 10^{-5} for all quantities solved. This number, in general, increases from RANS towards PANS. Additionally, for EARSM the anisotropy tensor has to be extra calculated and has a strong influence on the iterative convergence of the momentum equations, and LCTM (not shown in Table 5) solves two more transport equations. Therefore, all approaches tested are more computationally expensive than RANS using the SST model. Note also that in the context of the segregated SIMPLE method employed, the pressure equation needs also more iterations to achieve the convergence tolerance when using EARSM, LCTM or SRS approaches.

- Table 6 shows rough estimates of computational times for case 1 and case 2. The results are estimated for MARIN `Marclus4` 2014 HPC cluster (each computational node has 2 Xeon(R) CPU E5-2660-v3-2.60GHz 10-cores CPUs, and an HBA Infiniband for inter-nodal communication). The results indicate that, for the same total simulation time, RANS-EARSM calculations are more expensive than RANS-SST but less than SRS, and that PANS-SRS calculations are more expensive than DDES ones. The RANS computational times here shown are obviously exaggerated, since in this case usually 150 time-units are enough to have statistic convergence in time-averaged quantities. However, for SRS calculations, simulation times larger than 300 time-units were imperative for the present test cases. For EARSM, shorter simulation times are usually needed than for SRS, but more research is needed before general guidelines can be made.

Model	Case 1	Case 2	Case 3	Case 4
RANS	22	7	14	21
EARSM	32	-	40	32
DDES	33	9	-	32
XLES	34	10	-	-
PANS	35	12	39*	-

Table 5: Averaged number of iterations per time step as a function of case and mathematical model. * denotes $f_k = 0.50$ instead of $f_k = 0.25$.

Case	Case 1					Case 2				
Model	$T_{\Delta t}$ [s]	T_{sim}	N_p	Cpu [d]	$CoreDays$	$T_{\Delta t}$ [s]	T_{sim}	N_p	Cpu [d]	$CoreDays$
RANS	36	500	80	13.9	1115.6	10	500	300	38.6	11574.1
EARSM	11	500	192	7.1	1363.5	–	–	–	–	–
DDES	44	500	80	17.0	1363.5	9	500	300	34.7	10416.7
XLES	40	500	80	15.5	1239.5	11	500	300	42.4	12731.5
PANS	23	500	80	22.3	1781.8	12	500	300	46.3	13888.9

Table 6: Estimated computational costs as a function of case and mathematical model. Computational time per time step, $T_{\Delta t}$, total simulation time, $T_{sim} = \Delta T V_\infty / D$ (see Table 1), number of processes, N_p, wall-clock time, Cpu, and total core-days computational time, $CoreDays$. Estimates for MARIN `Marclus4` 2014 HPC cluster.

5 CONCLUSIONS

This study investigates the modelling accuracy of RANS and SRS models to simulate shear-layer flows around blunt bodies. The selected formulations are the isotropic RANS $k-\omega$ SST with or without the LCTM, an anisotropic RANS EARSM, DDES, XLES and PANS. These models were assessed on four cases: the flow past a circular cylinder at Re of 3,900 and 140,000, and the flow around a rounded square prism at $Re = 100,000$ and angles of incidence of 0 and 45 degrees. The outcome of the present study leads to the following conclusions:

- The modelling accuracy of traditional isotropic RANS models is insufficient to simulate the class of flows addressed in this study.
- The EARSM model used in this investigation leads to a substantial improvement of the quality of RANS simulations. For boundary-layer transition-dominated flows, the usage of LCTM transition models also improves the RANS results.
- In general, the SRS models tested in this work show a good agreement with the experiments, specially for the two first cylinder cases. For the rounded square prism case more research is needed.
- The application of hybrid formulations such as DDES or XLES is not justified if boundary-layer transition phenomena are critical.
- The numerical demands of RANS increase significantly from the SST to the EARSM, and from the RANS/EARSM to the SRS tested, if one considers not only the computational costs per time-step but the total number of time-steps needed (total simulation time) to reach statistically converged results.

Further work is needed in order to finalize the complete assessment of theses models for the rounded square prism case. Currently, all turbulence approaches presented here are also being applied for flows around foils, 3D wings, cavitating propeller flows, offshore constructions, free-surface flows and manoeuvering ships. Verification and validation studies of all these cases will help to derive guidelines for the usage of these new turbulent approaches for maritime industry relevant flows.

ACKNOWLEDGMENTS

This research is partially funded by the Dutch Ministry of Economic Affairs. This support is gratefully acknowledged.

REFERENCES

[1] B. Cantwell and D. Coles. An Experimental Study of Entrainment and Transport in the Turbulent near Wake of a Circular Cylinder. *Journal of Fluid Mechanics*, Vol. **136**, pp. 321-374, 1983;

[2] H.S Dol, J.C. Kok, and B. Oskam. Turbulence Modelling for Leading Edge Vortex Flows. *In 40th AIAA Aerospace Sciences Meeting and Aerospace Exposition*, Reno, USA, 14-17 January, 2002;

[3] L. Eça, R. Lopes, G. Vaz, J. Baltazar, D. Rijpkema. Validation Exercises of Mathematical Models for the Prediction of Transitional Flows. *In 31st Symposium on Naval Hydrodynamics* Monterey, CA, USA, 11-16 September 2016;

[4] S. Girimaji. Partially-Averaged Navier-Stokes Model for Turbulence: A Reynolds-Averaged Navier-Stokes to Direct Numerical Simulation Bridging Method. *Journal of Applied Mechanics*, Vol. **73**(3), pp.413-421, 2006;

[5] M. Gritskevich, A. Garbaruk, J. Schtze, and F. Menter. Development of DDES and IDDES Formulations for the $k-\omega$ Shear Stress Transport Model. *Journal of Flow, Turbulence and Combustion*, Vol. **88**(3), pp.431-449, 2012;

[6] H. Jang, B. Koo, J.W. Kim. High Reynolds Number Workshop. *In 35th International Conference on Ocean, Offshore and Arctic Engineering*, Busan, South Korea, 15-17 June, 2016;

[7] J.C. Kok, H. Dol, and B. Oskam Extra-Large Eddy Simulation of Massively Separated Flows. *In 42nd AIAA Aerospace Sciences Meeting and Exhibit*, Reno, USA, 5-8 January, 2004;

[8] J.C. Kok. Resolving the Dependence on Freestream Values for the $k-\omega$ Turbulence Model. *AIAA Journal*, Vol. **38**(7), pp.1292-1295, 2000;

[9] R.B. Langtry, and F.R. Menter. Correlation-Based Transition Modeling for Unstructured Parallelized Computational Fluid Dynamics Codes. *AIAA Journal*, Vol. **47**(12), pp.2894-2906, 2009;

[10] F.R. Menter, M. Kuntz, and R. Langtry. Ten Years of Industrial Experience with the SST Turbulence Model. *In Turbulence, Heat and Mass Transfer 4*, Antalya, Turkey, 12-17 October, 2003;

[11] C. Mockett. Go4Hybrid: Grey Area Mitigation for Hybrid RANS-LES Methods. *In Go4Hybrid Final Workshop*, 28th 29th Sept 2015, Berlin, Germany;

[12] S. Nanda. Flow past a Square-Prism: A Numerical Study. *MSc Thesis*, TU Delft, May 2016;

[13] C. Norberg. Pressure Distributions Around a Circular Cylinder in Cross-Flow. *In 3rd Symposium on Bluff Body Wake and Vortex-Induced Vibrations (BBVIV3)*, Port Douglas, Australia, 17-20 December 2002;

[14] C. Norberg. Fluctuating Lift on a Circular Cylinder: Review and New Measurements. *Journal of Fluids and Structures*, Vol. **17**(1), pp. 59-96, 2003;

[15] P. Parnaudeau, J.C.D. Heitz, and E. Lamballais. Experimental and Numerical Studies of the Flow over a Circular Cylinder at Reynolds Number 3900. *Physics of Fluids*, Vol. **20**(8), 085101, 2008;

[16] F.S. Pereira, G. Vaz, and L. Eça. On the Numerical Requirements of RANS and Hybrid Turbulence Models. *In VI International Conference on Computational Methods in Marine Engineering (MARINE2015)*, Rome, Italy, 15-17 June, 2015;

[17] F.S. Pereira, G. Vaz, and L. Eça. An Assessment of Scale-Resolving Simulation Models for the Flow Around a Circular Cylinder. *In Turbulence Heat and Mass Transfer 8 (THMT15)*, Sarajevo, Bosnia Herzegovina, 15-18 September, 2015;

[18] F.S. Pereira, G. Vaz, and L. Eça. An Assessment of Numerical and Modelling Errors for a Rounded-Corner Cylinder at High Reynolds Number. *In 37th International Conference on Ocean, Offshore & Arctic Engineering*, Busan, South Korea, 19-24 June, 2016;

[19] F.S. Pereira, G. Vaz, L. Eça, S. Lemaire. On the Numerical Prediction of Transitional Flows With Reynolds-Averaged Navier-Stokes and Scale-Resolving Simulation Models. *In 35th International Conference on Ocean, Offshore and Arctic Engineering*, Busan, South Korea, 19-24 June, 2016;

[20] F.S. Pereira, L. Eça, G. Vaz. Verification and Validation Exercises for the Flow Around the KVLCC2 Tanker at Model and Full-Scale Reynolds Numbers. *Ocean Engineering*, Vol. **129**, pp. 133-148, 2017;

[21] F.S. Pereira, G. Vaz, L. Eça, and S.S. Girimaji. Simulation of the Flow Around a Circular Cylinder at $Re = 3900$ with Partially-Averaged Navier-Stokes Equations. *Submitted to the International Journal of Heat and Fluid Flow*;

[22] F.S. Pereira, G. Vaz, L. Eça. Evaluation of RANS and SRS Models for the Simulation of the Flow Around a Circular Cylinder. *Submitted to the International Journal of Heat and Fluid Flow*;

[23] A. Roshko. Experiments on the Flow past a Circular Cylinder at Very High Reynolds Number. *Journal of Fluid Mechanics*, Vol. **10**(3). pp. 345-356, 1961.

[24] G. Rosetti. Improvements in the Numerical Modeling of Turbulence and Fluid-Structure Interaction for the Vortex-Induced Vibrations of a Rigid Cylinder. *PhD Thesis*, University of Sao Paolo, Brazil, June 2015;

[25] G. Vaz, F. Jaouen, M. Hoekstra. Free-Surface Viscous Flow Computations: Validation of URANS Code FreSCo. *In 28th International Conference on Ocean, Offshore and Arctic Engineering*, Honolulu, Hawaii, USA, May 31-June 5, 2019.